



# Roles of Polarization and Detuning in the Noise-induced Relaxation Dynamics of Atomic-Molecular Bose Condensates

Avinaba Mukherjee <sup>1,\*</sup> and Raka Dasgupta <sup>1,†</sup>

<sup>1</sup>*Department of Physics, University of Calcutta, 92 A. P. C. Road, Kolkata 700009, India*

(Dated: December 2, 2025)

We study the relaxation process of a resonant Bose gas under the influence of Gaussian white noise. We characterize the system dynamics in terms of the polarization or imbalance between the atoms and molecules, and the system coherence. The relaxation times corresponding to these two quantities are studied both using a mean-field model, and a Born Green Kirkwood Yvon hierarchy that takes into account the higher-order correlations. The role of the initial polarization and the Feshbach detuning are investigated. It is found with an increasing initial population imbalance, the longitudinal relaxation time (that governs the dynamics of the polarization) grows, while the transverse relaxation time (that governs the dynamics of the coherence) decays. As for the varying Feshbach detuning, it is observed that the longitudinal relaxation time reaches its minima and its transverse counterpart reaches its maxima near the resonance. We also study how the initial polarization and the detuning affect physical quantities like drift speed, condensate fraction, fidelity and entanglement entropy etc, and find the results to be fully consistent with the behavior of the relaxation dynamics of the system.

## I. INTRODUCTION

A coupled system of atomic and molecular Bose-Einstein condensates (BECs) has emerged as a fascinating platform, drawing significant attention and hosting various exciting quantum-statistical phenomena, in recent years [1–16]. In this hybrid system, two atomic bosons may merge to form a molecular boson through a Feshbach resonance mechanism [17, 18]. This setup effectively mirrors the behavior of a Bosonic Josephson junction [19–38], where atom-molecule coupling serves an analogous role to tunneling in traditional Josephson junctions. Here, the atomic (A-BEC) and molecular (M-BEC) condensate states are energetically separated by a formation threshold similar to the insulating barrier in a typical Josephson junction. This energy threshold becomes a crucial, tunable parameter governing the system’s behavior.

The study of non-equilibrium dynamics for Bosonic double-well has gained significant relevance [39–44]. In the presence of Gaussian white noise that affects the amplitude of hopping and detuning, the Bosonic Josephson Junction exhibits damped oscillations of population imbalance and relative phase, relaxing toward a steady state [45]. Incorporating quantum fluctuations beyond the Mean Field (MF) approach using the Bogoliubov backreaction (BBR) formalism reveals that even in the absence of noise and at zero temperature ( $T = 0$ ), single-particle coherence deteriorates due to many-body entanglement [46]. Although the MF approximation adequately captures short-time relaxation, accurate modelling over longer time scales, especially under phase noise, necessitates the BBR method for such bimodal atom-molecule conversion systems [47].

In our recent work [48], we investigated how population imbalance or polarization and quantum coherence evolve towards equilibrium using the MF and BBR approaches, with the initial variances serving as a key parameter, particularly when noise perturbs both the coupling strength and the de-

tuning. The full dynamics of the system is described by the Bloch vector components:  $\hat{L}_x$ ,  $\hat{L}_y$ , and  $\hat{L}_z$ . While both approaches exhibit damped oscillations under noise, their relaxation times differ significantly. These disparities stem from higher-order self-correlated and cross-correlated fluctuations among the Bloch vector components. The characteristic relaxation times ( $T_x$ ,  $T_y$ , and  $T_z$ ) for each Bloch component are influenced by the variances and covariances of  $\hat{L}_x$ ,  $\hat{L}_y$ , and  $\hat{L}_z$ , while the initial imbalance and detuning are held constant.

In this manuscript, we investigate how the initial population imbalance ( $|s_z^0|$ ) and detuning ( $\epsilon_b$ ) influence the relaxation times associated with both coherence and population imbalance. To interpret these findings, we analyze several physical observables (i) drift speed ( $|\dot{s}_z|$ ), (ii) von Neumann entropy ( $S_v$ ), (iii) fidelity ( $F$ ), and (iv) the Husimi  $Q$  distribution ( $H$ ), which help to explain the behavior of relaxation times when  $|s_z^0|$  treated as the variable.

Additionally, to provide physical insight into the behind the behaviour of relaxation times as functions of detuning, we present several indicators: (i) conversion-efficiency ( $\Gamma$ ), (ii) participation-ratio ( $P_R$ ), (iii) the condensate fraction ( $C_+$ ), and (iv) quantum-fisher-information ( $Q$ ) while  $\epsilon_b$  serve as a variable. Near the resonance point, all the time-averaged these physical quantity attain their maximum value.

This paper is organized as follows. Sec. II presents the foundational model, derives the governing dynamics, and details the influence of noise. Sec. III focuses on the relaxation processes within both the MF and BBR descriptions. Sec. IV is devoted to setting up experimentally realizable parameters. Sec. V analyzes the dependence of the longitudinal and transverse relaxation times on the Feshbach detuning ( $\epsilon_b$ ) and the initial polarization ( $|s_z^0|$ ). In Sec. VI, we identify several signatures that are consistent with the behavior of both longitudinal ( $T_z$ ) and transverse ( $T_{x-y}$ ) relaxation times. Finally, Sec. VII summarizes our conclusions.

## II. BASIC HAMILTONIAN FRAMEWORK AND NOISE EFFECTS

We study a system in which two bosonic atoms can coherently bind to form a bosonic molecule through the mechanism of Feshbach resonance [49–51]. In this resonance phenomenon, the underlying physics is captured by a two-channel model, comprising an open (or entrance) channel and a closed channel [52]. When the energy level of the open channel aligns with that of the closed channel, a resonant coupling occurs, allowing two free atoms to form a bound molecular state i.e., a bosonic dimer. The energy gap between the A-BEC and the M-BEC is denoted by  $\epsilon_b$ . This resonance condition can be precisely controlled by varying an external magnetic field, effectively tuning the relative energies of the two channels. The dynamics of this coupled atom-molecule system governed by the following Hamiltonian: [53–56].

$$\hat{H} = \frac{u_1}{2} \hat{a}^\dagger \hat{a}^\dagger \hat{a} \hat{a} + \frac{u_2}{2} \hat{b}^\dagger \hat{b}^\dagger \hat{b} \hat{b} + u_3 \hat{a}^\dagger \hat{b}^\dagger \hat{b} \hat{a} + g(\hat{a}^\dagger \hat{a}^\dagger \hat{b} + \hat{b}^\dagger \hat{a} \hat{a}) + \epsilon_b \hat{b}^\dagger \hat{b} \quad (1)$$

In this framework,  $\hat{a}^\dagger$  and  $\hat{a}$  denote the creation and annihilation operators for bosonic atoms, respectively, while  $\hat{b}^\dagger$  and  $\hat{b}$  serve as the corresponding operators for bosonic molecules. The parameters  $u_1$  and  $u_2$  characterize the interaction strengths between atoms and between molecules, respectively. The term  $u_3$  accounts for the interaction between atomic and molecular bosons. The coupling constant  $g$  quantifies the strength of the Feshbach resonance that facilitates the conversion between atomic and molecular states.

In Sec. II A, we express the system Hamiltonian through the components of the Bloch vector, enabling us to explore the coherent evolution of the system. Following this, in Sec. II B, we incorporate Gaussian white noise into both the coupling strength and the detuning term.

### A. Two state model

To facilitate visualization, we adopt a Bloch vector representation analogous to that used in spin systems. Our focus lies on a two-state model, where the relevant basis states are the fully molecular state and the fully atomic state, which are mapped onto the North ( $|1\rangle$ ) and South ( $|0\rangle$ ) poles of the Bloch sphere, respectively in Fig. (1). Unlike conventional spin systems, however, the components of the Bloch vector in this context do not satisfy the standard SU(2) algebra [57–59].

We define the components of the Bloch vector, also known as Schwinger pseudo-spin operators [60, 61], as follows [47, 48, 62]:  $\hat{L}_x = \sqrt{2}(\hat{a}^\dagger \hat{a}^\dagger \hat{b} + \hat{b}^\dagger \hat{a} \hat{a})/N^{3/2}$ ,  $\hat{L}_y = \sqrt{2}i(\hat{a}^\dagger \hat{a}^\dagger \hat{b} - \hat{b}^\dagger \hat{a} \hat{a})/N^{3/2}$ ,  $\hat{L}_z = (2\hat{b}^\dagger \hat{b} - \hat{a}^\dagger \hat{a})/N$ , and  $N = 2\hat{b}^\dagger \hat{b} + \hat{a}^\dagger \hat{a}$

In this formulation,  $\hat{L}_x$  and  $\hat{L}_y$  correspond to the real and imaginary components of the coherence between the atomic

and molecular states, respectively, while  $\hat{L}_z$  quantifies the population imbalance between atoms and molecules [63]. The total number of atoms in the system is denoted by  $N$ . The relevant commutation relations among the Bloch vector components, which are essential for analyzing the dynamics of system, are listed in [47, 48, 64]. We define the rescaled interaction parameters as  $U_1 = Nu_1$ ,  $U_2 = Nu_2$ ,  $U_3 = Nu_3$ , and the effective coupling strength as  $\tilde{g} = g\sqrt{N}$ . The interaction strengths are given by  $u_1 = 4\pi\hbar^2 a_{bg}/m_{\text{atom}}$ ,  $u_2 = 4\pi\hbar^2 a_{bb}/m_{\text{molecule}}$ , and  $u_3 = 4\pi\hbar^2 a_{ab}/\mu$ , where  $a_{bg}$  and  $a_{bb}$  are the background scattering lengths of the bosonic atom and molecule, respectively, and  $a_{ab}$  denotes the atom-molecule scattering length. The coupling constant  $g$  is defined as  $g = \sqrt{\mu_{\text{co}} \Delta B} u_1$ , where  $\mu_{\text{co}}$  is the magnetic moment of the bosonic atom, and  $\Delta B$  is the resonance width. The reduced mass of the atom-molecule pair is  $\mu = m_a m_b / (m_a + m_b)$ , where  $m_{\text{atom}}$  and  $m_{\text{molecule}}$  are the atomic and molecular masses, respectively. The binding energy is given by  $\epsilon_b = \mu_{\text{co}}(B - B_0)$ , with  $B$  being the externally applied magnetic field and  $B_0$  the position of the Feshbach resonance.

### B. Impact of Noise on the Basic Hamiltonian

Stochastic noise terms now perturb the modified coupling strength  $\tilde{g}$  and detuning  $\epsilon_b$ . These noise processes have zero mean and delta correlated [65]. In this framework, condensed particles are constitute the system, while non condensed (thermal) particles act as the surrounding bath [66, 67]. The coupling noise strength originates from decoherence or dephasing processes arising due to elastic collisions between the thermal cloud and the BECs [68]. In contrast, noise strength in  $\epsilon_b$  stems from fluctuations in the applied magnetic field near the Feshbach resonance [57] or from thermal fluctuations in the BEC at finite temperatures [69].

In the next section (Sec. III), we explore how the Bloch vector components relax in both the thermodynamic (mean-field) and quantum (Bogoliubov backreaction) frameworks.

## III. DYNAMICAL EQUATIONS

In Sec. III A, we analyze the mean-field (MF) and beyond-mean-field (BBR) dynamics of the Bloch vector components. In Sec. III B, we establish an analogy between the MF and BBR regimes with the strong and weak coupling limits. Finally, in Sec. III C, we show that among all the variance terms,  $\Delta_{zz}$  leads to maximum fluctuation. As a result, the relaxation time is difficult to calculate in presence of  $\Delta_{zz}$ .

### A. Mean field and Bogoliubov backreaction

In this section, we focus on the relaxation dynamics of the Bloch vector components. We begin by analyzing the system using the MF approach, which involves only the first mo-

ments of the Bloch vector components. We then extend our analysis to include the effects of non-zero variance and covariance, capturing higher-order correlations through the BBR method. Under the Gaussian (coherent-state) approximation, operator products factorize as  $\langle \hat{L}_i \hat{L}_j \rangle = \langle \hat{L}_i \rangle \langle \hat{L}_j \rangle$  [46]. Defining  $s_i = \langle \hat{L}_i \rangle$  ( $i = x, y, z$ ), we go beyond the MF limit using the BBR method, which includes second-order moments to capture correlations and quantum fluctuations. Specifically, a second-order truncation of the Bogoliubov Born Green Kirkwood Yvon (BBGKY) hierarchy is employed, wherein three operator expectations are approximated as:

$$\langle \hat{L}_i \hat{L}_j \hat{L}_k \rangle \approx \langle \hat{L}_i \hat{L}_j \rangle \langle \hat{L}_k \rangle + \langle \hat{L}_i \rangle \langle \hat{L}_j \hat{L}_k \rangle + \langle \hat{L}_i \hat{L}_k \rangle \langle \hat{L}_j \rangle - 2 \langle \hat{L}_i \rangle \langle \hat{L}_j \rangle \langle \hat{L}_k \rangle \quad (2)$$

Moreover, we define the two-point correlation function  $\Delta_{ij}$  as follows:

$$\Delta_{ij} = \langle \hat{L}_i \hat{L}_j + \hat{L}_j \hat{L}_i \rangle - 2 \langle \hat{L}_i \rangle \langle \hat{L}_j \rangle \quad (3)$$

When  $\Delta_{ij} \neq 0$ , the system lies in the BBR regime, reflecting the presence of nontrivial correlations. In contrast,  $\Delta_{ij} = 0$  corresponds to the MF regime, where the system evolves within the eigenstates of the relevant observable [70]. Equivalently, vanishing variance or covariance indicates that the observable coincides with its mean value, signifying an eigenstate of the system. In typical experimental setups [71, 72], a large number of particles are trapped. By incorporating both first- and second-order moments in the large- $N$  limit, the system dynamics can be constructed as:

$$\dot{s}_x = c_1(\Delta_{yz} + 2s_y s_z) + c_2 s_y - \frac{\gamma_z s_x}{2} \quad (4a)$$

$$\begin{aligned} \dot{s}_y = & -c_1(\Delta_{zx} + 2s_z s_x) - c_2 s_x - \frac{\tilde{g}}{\sqrt{2}}(1 + 2s_z - \frac{3}{2}\Delta_{zz} - 3s_z^2) \\ & + \gamma_x(-2s_y + 3\Delta_{yz} + 6s_y s_z) - \frac{\gamma_z s_y}{2} \end{aligned} \quad (4b)$$

$$\dot{s}_z = 2\sqrt{2}\tilde{g}s_y - \gamma_x(1 + 2s_z - \frac{3}{2}\Delta_{zz} - 3s_z^2) \quad (4c)$$

$$\dot{\Delta}_{xx} = 4c_1 s_y \Delta_{zx} + 2(2c_1 s_z + c_2) \Delta_{xy} - \gamma_z \Delta_{xx} \quad (4d)$$

$$\begin{aligned} \dot{\Delta}_{yy} = & \left( -4c_1 s_x - 2\sqrt{2}\tilde{g}(1 - 3s_z) + 12\gamma_x s_y \right) \Delta_{yz} \\ & - 2(2c_1 s_z + c_2) \Delta_{xy} - \left( \gamma_z + 4\gamma_x(1 - 3s_z) \right) \Delta_{yy} \end{aligned} \quad (4e)$$

$$\dot{\Delta}_{zz} = 4\sqrt{2}\tilde{g}\Delta_{yz} - 4\gamma_x(1 - 3s_z)\Delta_{zz} \quad (4f)$$

$$\begin{aligned} \dot{\Delta}_{xy} = & -(2c_1 s_z + c_2) \Delta_{xx} + (2c_1 s_z + c_2) \Delta_{yy} + 2c_1 s_y \Delta_{yz} \\ & + \left( 6\gamma_x s_y - 2c_1 s_x - \sqrt{2}\tilde{g}(1 - 3s_z) \right) \Delta_{zx} \\ & - \left( \gamma_z + 2\gamma_x(1 - 3s_z) \right) \Delta_{xy} \end{aligned} \quad (4g)$$

$$\begin{aligned} \dot{\Delta}_{yz} = & \left( -2c_1 s_x - \sqrt{2}\tilde{g}(1 - 3s_z) + 6\gamma_x s_y \right) \Delta_{zz} - (2c_1 s_z + c_2) \Delta_{zx} \\ & + 2\sqrt{2}\tilde{g}\Delta_{yy} - \left( \frac{\gamma_z}{2} + 4\gamma_x(1 - 3s_z) \right) \Delta_{yz} \end{aligned} \quad (4h)$$

$$\begin{aligned} \dot{\Delta}_{zx} = & 2c_1 s_y \Delta_{zz} + (2c_1 s_z + c_2) \Delta_{yz} + 2\sqrt{2}\tilde{g}\Delta_{xy} \\ & - \left( 2\gamma_x(1 - 3s_z) + \frac{\gamma_z}{2} \right) \Delta_{zx} \end{aligned} \quad (4i)$$

When only individual fluctuations ( $\Delta_{ii}^0$ ) or pairwise correlations ( $\Delta_{ij}^0$ ) are present, the relaxation times can either increase or decrease relative to MF values, depending on the specific configuration and interplay of correlations. It is a closed system because the total number of particles ( $\dot{N} = 0$ ) is conserved, as shown in Appendix A.

## B. Classical analogy

Consider a classical system consisting of three springs and two bobs, where each bob is connected to its respective stand via a spring. In addition, the two bobs are interconnected by an intermediate spring. If the spring constant of the intermediate spring is equal to that of the two boundary springs, the system is in the strong coupling limit, where energy is rapidly transferred between the bobs. In contrast, if the intermediate spring has a much lower spring constant than the boundary springs, energy transfer between the bobs occurs more slowly, a phenomenon known as the weak coupling limit. When the middle spring is compressed or stretched, an anti-symmetric mode appears, as illustrated in Fig. (2) [73, 74]. The constructive (waxing) and destructive (waning) interference of the two bobs occur at specific instants [75]. If red bob and blue bob move toward the left and right, respectively, the outer springs are stretched, while the inner spring is compressed twice [76]. As shown in Fig. (2), both  $N_a$  and  $2N_b$  contribute to forming a quasi-standing wave [77, 78], where the sum of the two determines the rapidly oscillating frequency, while their difference governs the slowly oscillating envelope. As the study involves the number oscillations of both A-BEC and M-BEC ( $N_a$ ) and ( $2N_b$ ), the red and blue blobs are depicted with nearly equal sizes. Strong and weak coupling correspond to the MF and BBR conditions, respectively. Here, the amplitudes are time-dependent [73], and in the weak coupling regime, an envelope forms around the rapidly oscillating spring, a phenomenon known as a beat [76].

## C. Nature of fluctuations

By taking higher-order time derivatives of Eqs. (4a), (4b), and (4c), we obtain a set of coupled, forced-damped oscillatory equations [79, 80] governing the dynamics of all Bloch vector components  $s_i$ .

$$\ddot{s}_i + \lambda_i \dot{s}_i + \omega_i^2 s_i = F_i \quad \text{while} \quad i \in \{x, y, z\} \quad (5a)$$

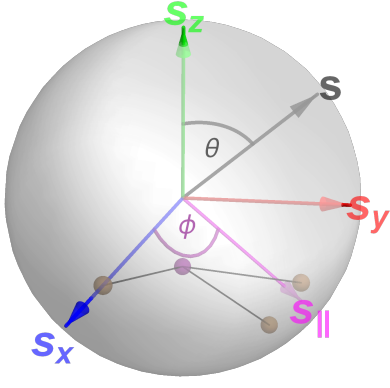


FIG. 1: A few initial states (brown) and the final equilibrium point (purple, south pole oriented state) are indicated on the Bloch sphere, where  $\theta$  and  $\phi$  denote the polar and azimuthal angles, respectively.

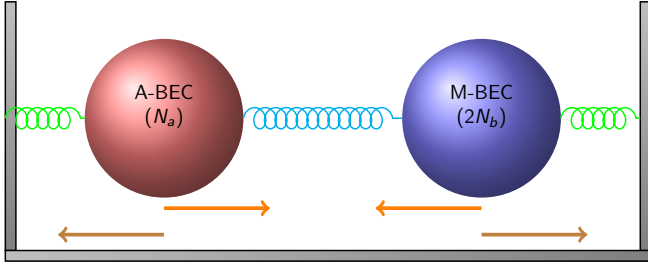


FIG. 2: Two types of outward motions for A-BEC ( $N_a$ ) and M-BEC ( $2N_b$ ).

where the damping rates ( $\gamma_i$ ), frequencies ( $\omega_i$ ), and forces ( $F_i$ ) are defined as follows:

$$\gamma_x = \text{constant}, \quad \gamma_y = f(s_z), \quad \gamma_z = f(s_z) \quad (5b)$$

$$\omega_x^2 = f(s_z, \Delta_{zz}), \quad \omega_y^2 = f(s_i, \Delta_{zz}), \quad \omega_z^2 = f(s_i, \Delta_{zz}) \quad (5c)$$

$$\begin{aligned} F_x &= f(s_y, s_z, \Delta_{yy}, \Delta_{zz}, \Delta_{zx}), \\ F_y &= f(s_z, \Delta_{yy}, \Delta_{zz}, \Delta_{xy}, \Delta_{zx}), \\ F_z &= f(s_x, s_y, \Delta_{zz}, \Delta_{yz}, \Delta_{zx}) \end{aligned} \quad (5d)$$

From Eq. (5d), we show that  $F_i$  are intrinsically generated forces, not external drives, since they depend only on the first and second moments of the Bloch-vector components.

The effective frequency ( $\omega_i^{\text{eff}}$ ) of under-damped ( $\lambda_i/\omega_i < 1$  [81]) force oscillation can be formed from Eq. (5a),

$$\omega_i^{\text{eff}} = \sqrt{\omega_i^2 - \frac{\lambda_i^2}{4}} \quad (6)$$

So,  $\omega_i^2$  can make contribution on  $\lambda_i$  [73, 75–77]. Detailed expressions of  $\omega_i^2$ ,  $\lambda_i$ , and  $F_i$  are placed in Appendix B. Here,

we observe that  $\omega_i$  depends only on a single type of variance ( $\Delta_{zz}$ ). Consequently,  $\omega_i^{\text{eff}}$  also depends on  $\Delta_{zz}$ . Thus, the presence of large  $\Delta_{zz}$  leads to an immensely fluctuating system dynamics. We therefore exclude it from all relaxation-time plots presented in Figs. (3) - (6).

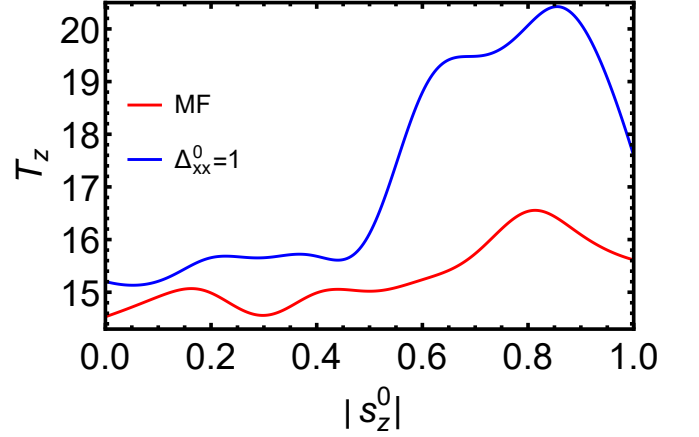


FIG. 3: Effect of absolute initial polarization ( $|s_z^0|$ ) variation with longitudinal relaxation time ( $T_z$ ) where MF (—), and  $\Delta_{xx}^0$  (—) are denoted by their respective colors.

In the next section (Sec. IV), we specify the initial conditions of the system and the experimental parameters used to study its dynamics.

#### IV. RELAXATION PROCESS

In Sec. IV A, we specify the initial conditions adopted for our study. Sec. IV B aims to determine the essential parameters of our system.

##### A. Choice of initial state

The resulting Bloch equations closely resemble those found in nuclear magnetic resonance (NMR) systems [82, 83]. The coherent dynamics of the Bloch vector components follow the Heisenberg equation of motion [61]. Initial condition for the Bloch vector components can be obtained in the following semiclassical form:  $\hat{L}_x = (1 - \tilde{z})\sqrt{1 + \tilde{z}}\cos\tilde{\phi}/\sqrt{2}$ ,  $\hat{L}_y = (1 - \tilde{z})\sqrt{1 + \tilde{z}}\sin\tilde{\phi}/\sqrt{2}$ , and  $\hat{L}_z = \tilde{z}$  where we specify the initial conditions for the Bloch vector components as  $s_x^0 = 0.707$ ,  $s_y^0 = 0$ , and  $s_z^0 = 0$ , corresponding to the phase-space values  $\tilde{z} = 0$  and  $\tilde{\phi} = 0$  which generates the Josephson 0-state [69, 84]. In Fig. (1), the initial state is indicated by a brown ball, whereas the final equilibrium state, depicted by a purple atom-heavy ball. The quantities  $s$  and  $s_{\parallel}$  denote the Bloch vector and its projection onto the equatorial plane, respectively. In this formulation, the atomic and molecular populations,  $N_a$  and  $N_b$ , are identified with the number operators  $\hat{a}^\dagger\hat{a}$  and  $\hat{b}^\dagger\hat{b}$ , respectively. The population polarization is given

by  $\tilde{z} = 2\hat{b}^\dagger\hat{b} - \hat{a}^\dagger\hat{a}$ , and the relative phase between the atomic and molecular BECs is  $\tilde{\phi} = 2\theta_a - \theta_b$ . These quantities are illustrated in the non-rigid pendulum model. This two-mode system is mapped onto a classical phase space, where  $\tilde{z}$  and  $\tilde{\phi}$  form a pair of canonically conjugate variables [63]. In this manuscript, the initial values of all variances and covariances are chosen as  $\Delta_{ii}^0 = \Delta_{ij}^0 = 1$ .

## B. Experimental parameters

For numerical solutions, we consider physical parameters corresponding to  $^{87}\text{Rb}$ . In particular, we adopt the experimentally measured values  $\Delta B = 0.21$  Gauss and  $B_0 = 1007.4$  Gauss [18], and set  $|B - B_0| = 10$  Gauss. Based on this choice, the system parameters are assigned as follows:  $U_1 = 1$ ,  $U_2 = 2$ ,  $U_3 = -1.5$ ,  $\tilde{g} = 0.2$ , and  $\epsilon_b = 2$  [18, 85–87]. We further define the coefficients  $c_1 = U_3/2 - U_1/2 - U_2/8$  and  $c_2 = U_1 - U_2/4 - \epsilon_b$ . In our case, these evaluate to  $c_1 = c_2 = -1.5$ . The noise strengths are set as fractions of the coupling and detuning:  $\gamma_x = 0.02$ , and  $\gamma_z = 0.2$ .

In Sec V, we demonstrate the behaviour of both longitudinal and transverse relaxation time as a function of initial polarization ( $|s_z^0|$ ) and Feshbach detuning ( $\epsilon_b$ ).

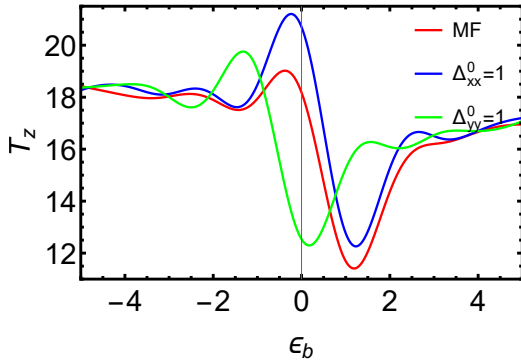


FIG. 4: Effect of activation of variance ( $\Delta_{ii}^0$ ) on longitudinal relaxation time ( $T_z$ ) driven by detuning ( $\epsilon_b$ ) variation where MF (—),  $\Delta_{xx}^0$  (—), and  $\Delta_{yy}^0$  (—) are denoted by their respective colors.

## V. LONGITUDINAL AND TRANSVERSE RELAXATION TIME

In Sec. V A, we identify the stable equilibrium point through the Jacobian matrix formalism. In Sec. V B, we evaluate both  $T_z$  and  $T_{x-y}$ , where  $|s_z^0|$ , and  $\epsilon_b$  are treated as variables.

### A. Stability analysis

In the absence of noise ( $\gamma_x = \gamma_z = 0$ ), if  $\Delta_{ij} = 0$ , then from Eq. (4c) we obtain  $s_y = 0$  when  $\dot{s}_z = 0$ . Incidentally,  $s_y = 0$  also makes  $\dot{s}_x = 0$  in Eq. (4a). Furthermore, substituting  $s_y = 0$  and  $\dot{s}_y = 0$  into Eq. (4b) yields the condition  $2c_1 s_z + c_2 \neq 0$ , which leads to the solutions  $s_z = 1$  or  $s_z = -1/3$ . For these values of  $s_z$ , we obtain  $s_x = -\tilde{g}(s_z - 1)(s_z + 1/3)/\sqrt{2}(2c_1 s_z + c_2)$ . Since, the jacobian can be defined as [88],

$$J_{ij} = \frac{\partial s_i}{\partial s_j} \quad (7)$$

So, numerical solutions of Eq. (7) leads to an unstable equilibrium point,  $(0, 0, 1)$  with

$$\lambda_1 = -0.061 - 4.464i, \quad \lambda_2 = -0.061 + 4.464i \quad (8a)$$

and,  $\lambda_3 = 0.083$ ,

and a stable equilibrium point  $(0, 0, -1/3)$  with

$$\lambda_1 = -0.134 - 0.754i, \quad \lambda_2 = -0.134 + 0.754i \quad (8b)$$

and,  $\lambda_3 = -0.091$

The detailed derivations are presented in Appendix C. Now, the real parts of the complex-conjugate eigenvalues are negative in both Eqs. (8a) and (8b); therefore, both cases exhibit an inward spiral [89]. However, Eq. (8a) has one positive real eigenvalue,  $\lambda_3$ , which causes the system to diverge along that direction. In contrast,  $\lambda_3$  in Eq. (8b) is negative, so the system converges in all directions and yields a stable solution. Furthermore, the equilibrium point  $(0, 0, -1/3)$  is found to be stable (an attractor), indicating that the atom-heavy state is dynamically preferred.

### B. Logitudinal and transverse relaxation time

We assume an exponential decay governed by

$$s_i(t) = s_i^0 e^{-t/\tau}, \quad (9)$$

where  $\tau$  is the decay time constant and  $s_i^0$  is the initial amplitude. The time interval between two measurements is  $\Delta t = t_f - t_i$ . The exponential relaxation time is then approximated as

$$\tau_{\text{relax}} = \frac{\Delta t}{\ln\left(\frac{s_i^0}{s_i}\right)}. \quad (10)$$

With Eq. (10) as our basis, we compute the relaxation times  $T_z$  and  $T_{x-y}$  for varying initial polarization ( $|s_z^0|$ ) and detuning ( $\epsilon_b$ ). The longitudinal relaxation time  $T_z$  increases with the increase of absolute initial imbalance ( $|s_z^0|$ ), as demonstrated in Fig. (3). Since the system is trapped in an atom-dominated state,  $T_z$  becomes more significant; that is, the system takes



longer to relax. Actually,  $T_z$  is the time required to relax  $s_z$  from  $s_z^0$  to  $s_z^{\text{eq}}$ . Here, activation of  $\Delta_{xx}^0$  enhances  $T_z$  more than the usual MF limit. The condition  $s_z = -1/3$  corresponds to equal populations of A-BEC and M-BEC. Since  $(0, 0, -1/3)$  represents the stable equilibrium point within the MF regime, the longitudinal relaxation time  $T_z$  increases on both sides of  $s_z = -1/3$ . Close to the resonance point, the transition probability between the two states increases, leading to faster population relaxation. As a result, the  $T_z$  reaches its minimum near resonance point, as illustrated in Fig. (4). Since relaxation rates are additive, the overall decay process follows an exponential profile while the decay rates for the  $s_x$  and  $s_y$  components differ. Therefore, the effective decay rate in the anisotropic transverse ( $x$ - $y$ ) plane is best characterized by the harmonic mean [90, 91]:

$$T_{x-y} = \frac{2T_x T_y}{T_x + T_y} \quad (11)$$

Enhanced  $|s_z^0|$  allows  $T_{x-y}$  to decrease due to the effect of coherence decays. As a result, the transverse coherence time  $T_{x-y}$  decreases. This trend is illustrated in Fig. (5) where activation of  $\Delta_{yy}^0$  enhances the fall of  $T_{x-y}$  more than in the other two cases (MF and  $\Delta_{xx}^0 = 1$ ).

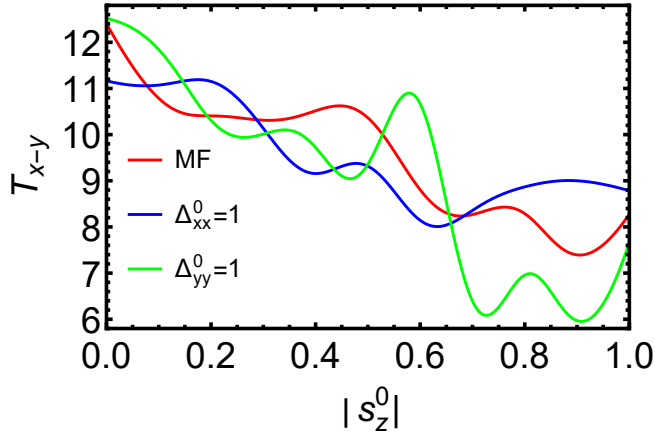


FIG. 5: Effect of absolute initial polarization ( $|s_z^0|$ ) variation with transverse relaxation time ( $T_{x-y}$ ) where MF (—),  $\Delta_{xx}^0$  (—), and  $\Delta_{yy}^0$  (—) are denoted by their respective colors.

Near resonance, the energy bias ( $\epsilon_b$ ) vanishes, leading to degenerate energy levels and thus enabling closed channel. In contrast, away from the resonance point, the appearance of the closed channel is difficult. More coherence observed near the equatorial plane, so coherence relaxation time increases near resonance.

Due to the rapid, wave-packet-like fluctuations observed in both  $T_{x-y}$  and  $T_z$ , the effect of  $\Delta_{zz}^0$  is excluded from Figs. (3) - (6). Besides, the effect of  $\Delta_{yy}^0$  is also excluded from Fig. (3).

In Sec. VI, we employ several markers as supporting circumstantial evidence to study the behavior of  $T_z$  and  $T_{x-y}$ .

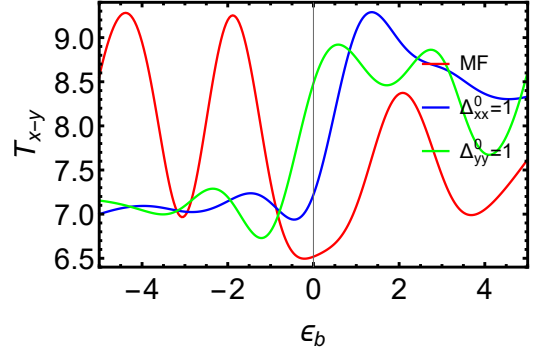


FIG. 6: Effect of activation of variance ( $\Delta_{ii}^0$ ) on transverse relaxation time ( $T_{x-y}$ ) when controlled through detuning ( $\epsilon_b$ ) variation where MF (—),  $\Delta_{xx}^0$  (—), and  $\Delta_{yy}^0$  (—) are denoted by their respective colors.

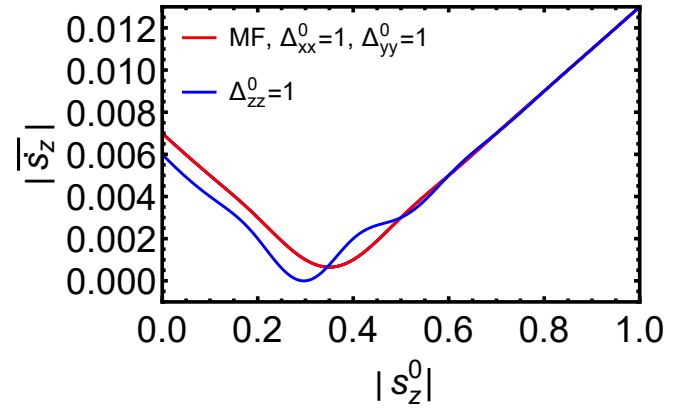


FIG. 7: Time-averaged drift speed ( $|\bar{s}_z|$ ) influenced by the absolute initial imbalance ( $|s_z^0|$ ). The effects of different initial variances  $\Delta_{ii}^0$  are indicated by the following colors: MF,  $\Delta_{xx}^0$ , and  $\Delta_{yy}^0$  (—), and  $\Delta_{zz}^0$  (—).

## VI. PROLONGED OR SLOW DOWN RELAXATION TIMES: EVIDENCE AND IMPLICATIONS

The time-averaged expectation of any operator  $\hat{A}$  is defined as [48]

$$\langle \hat{A} \rangle_t = \bar{A} = \frac{\int_{t_i}^{t_f} A(t) dt}{\int_{t_i}^{t_f} dt} \quad (12)$$

computed over  $t_i = 0$  to  $t_f = 50$ , the interval capturing the relaxation dynamics. Here,  $t_i = 0$  corresponds to equal population ( $s_z^0 = 0$ ), and beyond  $t_f = 50$ , fluctuations decay as the system approaches a steady atom-favored state. Although the system is not in equilibrium or steady state, and technically, not in the ergodic domain, still we use the time-averaging as it effectively characterizes the dominant behavior during relaxation.

In Sec. VIA, we investigate the effects of  $|s_z^0|$ , and  $\epsilon_b$  on a few relevant physical quantities and attempt to relate these findings to the trends observed in the relaxation process. Specifi-

cally, we focus on four key quantities: (i) time-averaged drift speed ( $|\bar{s}_z|$ ), (ii) time-averaged conversion efficiency ( $\bar{\Gamma}$ ) as an indicator for behaviour of  $T_z$  when  $s_z^0$ , and  $\epsilon_b$  are the variable, respectively. The behavior of  $T_{x-y}$  is consistently reflected in (i) the time-averaged von Neumann entropy ( $\bar{S}_V$ ), (ii) time-averaged fidelity ( $\bar{F}$ ), and (iii) the time-averaged Husimi- $Q$  distribution ( $\bar{H}$ ) when the initial polarization  $s_z^0$  is varied. Also, when the detuning  $\epsilon_b$  is treated as the variable, the (i) time-averaged participation ratio ( $\bar{P}_R$ ), (ii) time-averaged condensate fraction ( $\bar{C}_+$ ), and (iii) time-averaged quantum Fisher information ( $\bar{Q}$ ) serve as indicators of coherence, as discussed in Sec. **VIB**. Subsequently, Sec. **VIC** provides the physical insight underlying the shift of the resonance position toward positive detuning (i.e., to the right of the resonance point).

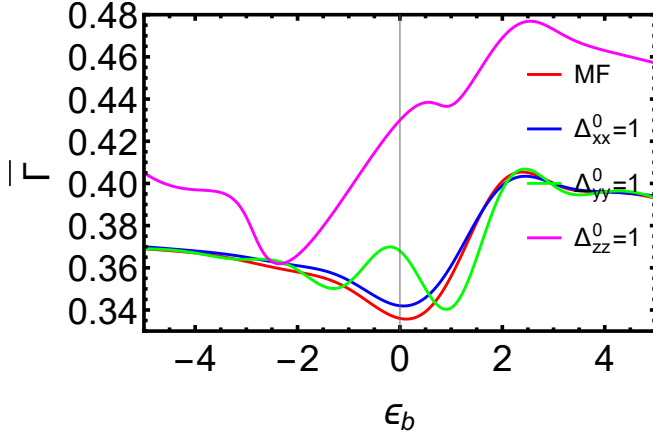


FIG. 8:

The time-averaged conversion-efficiency ( $\bar{\Gamma}$ ) is motivated by detuning ( $\epsilon_b$ ), where the following variances are represented by their respective colors: MF (—),  $\Delta_{xx}^0 = 1$  (—),  $\Delta_{yy}^0 = 1$  (—), and  $\Delta_{zz}^0 = 1$  (—).

### A. Longitudinal relaxation time

#### 1. Drift speed: A Quantitative Marker of Longitudinal Relaxation Time under Variable Initial Imbalance

An increase in  $|s_z^0|$  toward the atomic state drives  $\bar{s}_z$  from an oscillatory regime into a gradually frozen domain. In this process, the magnitude of  $|\bar{s}_z|$  initially decreases before increasing again, so that the corresponding relaxation time  $T_z$  effectively increases in Fig. (7).

#### 2. Probing Longitudinal Relaxation Time via Conversion Efficiency as a function of Feshbach detuning

Conversion efficiency is defined as,

$$\Gamma = \frac{2n_b}{N} = \frac{1 + s_z}{2} \quad (13)$$

In Fig. (8),  $\bar{\Gamma}$  reaches its maxima near resonance, as a result of this,  $T_z$  reaches its minima near the resonance position because transition from one state to other takes shorter time.

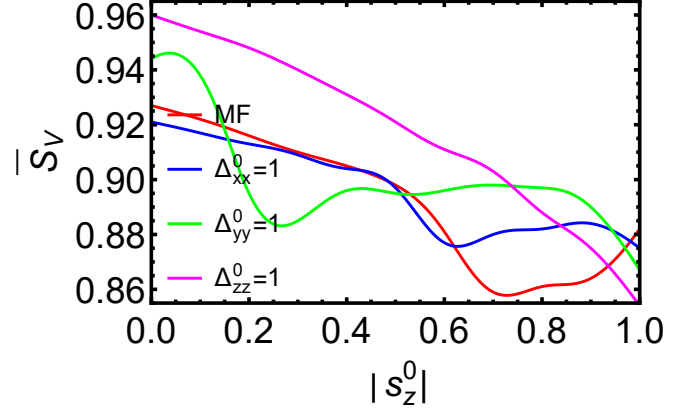


FIG. 9: The time-averaged von-neumann entropy ( $\bar{S}_V$ ) as a function of absolute initial imbalances ( $|s_z^0|$ ). The contributions from each variance are represented by the following colors: MF (—),  $\Delta_{xx}^0$  (—),  $\Delta_{yy}^0$  (—), and  $\Delta_{zz}^0$  (—).

### B. Transverse relaxation time

#### 1. Linking Von-neumann entropy to Transverse Relaxation under Variable Initial Imbalance

Here,  $\sigma_j$  are  $(2 \times 2)$  Pauli matrices. The density matrix can be represented as [92, 93]

$$\hat{\rho} = \frac{I + \sigma_j s_j}{2}, \quad \text{where } j \in x, y, z, \quad (14)$$

with  $\sigma_j$  denoting the  $(2 \times 2)$  Pauli matrices.

In matrix form, Eq. (14) takes the form:

$$\hat{\rho} = \frac{1}{2} \begin{pmatrix} 1 + s_z & s_x - i s_y \\ s_x + i s_y & 1 - s_z \end{pmatrix}. \quad (15)$$

Now, purity is defined as [94],

$$P = \text{Tr} \hat{\rho}^2 = \frac{1 + \sum_j s_j^2}{2} \quad (16)$$

which is reduced through the decoherence process. Here,  $P = 1$  corresponds to a pure state, while  $P = 1/2$  corresponds to a maximally mixed state.

The von Neumann entropy is given by [93]:

$$S_V(P) = - \frac{1 + \sqrt{2P-1}}{2} \log_2 \left( \frac{1 + \sqrt{2P-1}}{2} \right) - \frac{1 - \sqrt{2P-1}}{2} \log_2 \left( \frac{1 - \sqrt{2P-1}}{2} \right) \quad (17)$$

where  $S_V(P) = 0$  and  $S_V(P) = 1$  correspond to pure and maximally mixed states, respectively.

From Fig. (9), we observe that  $\bar{S}_V$  decrease as  $|s_z^0|$  increases, because the tendency of  $|s_z^0|$  toward a pure state enhances the loss of coherence. Furthermore, the evolution of the system toward a pure state (i.e., a fully atomic state) is indicative of  $\bar{S}_V$  reduction.

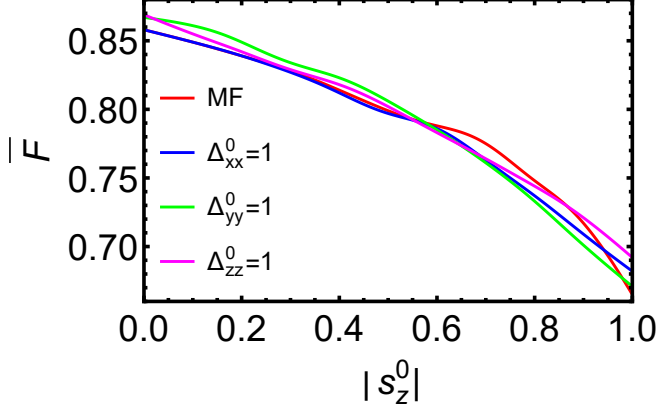


FIG. 10: Time-averaged fidelity ( $\bar{F}$ ) as a function of absolute initial imbalances ( $|s_z^0|$ ). The following colors represent the contributions from each variance: MF (—),  $\Delta_{xx}^0$  (—),  $\Delta_{yy}^0$  (—), and  $\Delta_{zz}^0$  (—).

## 2. Fidelity and the Transverse Relaxation Signature under Variable Initial Imbalance

If  $\hat{\rho}_1 = \hat{\rho}(t=0)$ , and  $\hat{\rho}_2 = \hat{\rho}(t)$  then Uhlmann Fidelity is defined as [95],

$$F = \left( \text{Tr} \sqrt{\sqrt{\rho_1} \rho_2 \sqrt{\rho_1}} \right)^2 = \text{Tr}(\rho_1 \rho_2) + 2 \sqrt{\det \rho_1 \det \rho_2} \quad (18a)$$

which recasts in terms of Bloch vector as

$$F = \frac{1 + \mathbf{s}(t=0) \cdot \mathbf{s}(t) + \sqrt{(1 - |\mathbf{s}(t=0)|^2)(1 - |\mathbf{s}(t)|^2)}}{2} \quad (18b)$$

where  $F$  measures overlap between the initial,  $\mathbf{s}(t=0)$  and final Bloch vector,  $\mathbf{s}(t)$ . In Fig. (10),  $\bar{F}$  decreases as a signature of loss of coherence when  $|s_z^0|$  runs in the extreme direction.

## 3. Elucidating Transverse Relaxation through Husimi-Q-distribution under Variable Initial Imbalance

If  $\theta$ , and  $\phi$  represent polar and azimuthal angle then Husimi Q-distribution [92, 96] and angular coordinate  $|\theta, \phi\rangle$  [94] are defined as

$$\begin{aligned} H(\theta, \phi) &= \frac{1}{\pi} \langle \theta, \phi | \hat{\rho} | \theta, \phi \rangle \\ &= \frac{1}{2\pi} (1 + s_z \cos \theta + s_x \sin \theta \cos \phi + s_y \sin \theta \sin \phi) \end{aligned} \quad (19a)$$

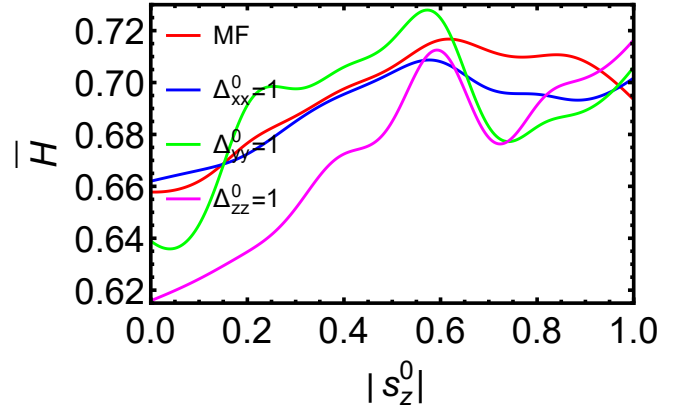


FIG. 11: Time-averaged Husimi-Q-distribution function ( $\bar{H}$ ) as a function of absolute initial imbalances ( $|s_z^0|$ ). The contributions from each variance are represented by the following colors: MF (—),  $\Delta_{xx}^0$  (—),  $\Delta_{yy}^0$  (—), and  $\Delta_{zz}^0$  (—).

where

$$|\theta, \phi\rangle = \cos \frac{\theta}{2} |0\rangle + e^{i\phi} \sin \frac{\theta}{2} |1\rangle \quad (19b)$$

As a signature of coherence loss also manifested with increasing  $\bar{H}$  in Fig. (11) with increasing  $|s_z^0|$ . If  $\bar{H}$  is azimuthally symmetric (i.e., independent of  $\phi$ ), then the system loses all of its coherence.

## 4. Assessing Transverse Relaxation through participation ratio as a function of Feshbach detuning

Now, purity ( $P$ ) [94] and participation-ratio ( $P_R$ ) [95] are related, where Inverse of Eq. (16) is called participation-ratio

$$P_R = \frac{2}{1 + \sum_j s_j^2} \quad (20)$$

Since,  $\epsilon_b$  breaks parity symmetry of energy, so,  $\bar{P}_R$  decreases as a signature of the system becoming more mixed or delocalized, i.e., more basis states participate near the resonance point in Fig. (12). In different words  $P_R$  can be defined as [97],

$$P_R = \sum_j |c_j|^4, \quad \text{where } j : \text{number of basis states} \quad (21)$$

For most coherent and pure states,  $P_R = 1/2$ , and 1 respectively in two mode system in Eq. (19b). Decreasing  $P_R$  means more coherence near the resonance point.



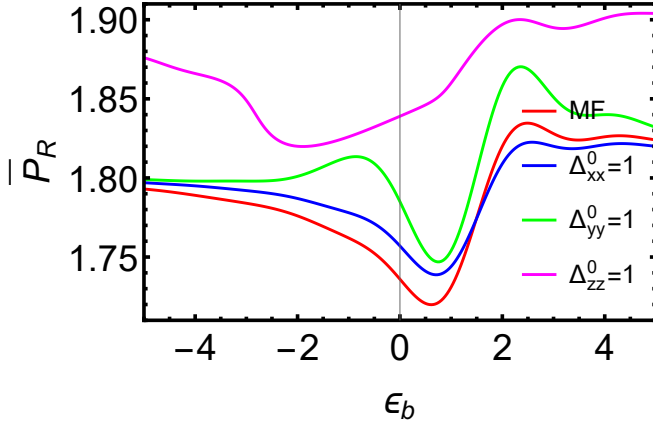


FIG. 12: Time-averaged participation-ratio ( $\bar{P}_R$ ) is controlled by detuning ( $\epsilon_b$ ) where the following variances are represented by their respective colors: MF (—),  $\Delta_{xx}^0 = 1$  (—),  $\Delta_{yy}^0 = 1$  (—), and  $\Delta_{zz}^0 = 1$  (—).

##### 5. Condensate fraction as an Indicator of Transverse Relaxation Dynamics as a function of Feshbach detuning

From, Eq. (15), we obtains these eigen values

$$C_{\pm} = \frac{1 \pm \sqrt{s_z^2 + 4\{s_x^2 + s_y^2 + (1 - s_z)(1 + 3s_z)\}}}{2} \quad (22)$$

Here, the diagonal elements represent atomic and molecular populations, while the off diagonal elements represent coherences. Here,  $C_{+}(-)$  [98] stands for the condensed and non-condensed parts. Near resonance position macroscopic coherence i.e.  $\bar{C}_{+}$ , reaches its maximum for all cases, as shown in Fig. (13).

##### 6. Quantum Fisher Information : The Fingerprint of Transverse Relaxation as a function of Feshbach detuning

Quantum Fisher Information ( $Q$ ) [99] is defined as,

$$Q = 4 \left( \left\langle \frac{\partial \psi}{\partial \phi} \middle| \frac{\partial \psi}{\partial \phi} \right\rangle - \left| \left\langle \frac{\partial \psi}{\partial \phi} \middle| \psi \right\rangle \right|^2 \right) \quad (23a)$$

If we use Eq. (19b) as  $|\psi\rangle$ , then,

$$Q = \sin^2 \theta \quad (23b)$$

If we use the unitary evolution on  $|\psi\rangle$  then we obtain [61]

$$|\psi\rangle_R = e^{-i\hat{n}} |\psi\rangle \quad (24a)$$

where,  $|\psi\rangle_R$  and  $\hat{n}$  are rotated wave vector and unit vector respectively which generates [100]

$$Q = \frac{4(\Delta_{xx} + \Delta_{yy} + \Delta_{zz})}{3} \quad (24b)$$

From, Eq. (15), we obtain the off-diagonal i.e.  $l_1$  norm or coherence ( $s_{||}$ ) [93],

$$s_{||} = |\rho_{12}| \propto \sin \theta \quad (25a)$$

So,

$$Q = s_{||}^2 \quad (25b)$$

$Q$  measures the parameter sensitivity. In Fig. (14),  $\bar{Q}$  reaches its maximum near resonance, i.e. parameter sensitivity is more prominent. As a result of this correlation or coherence increases [101].

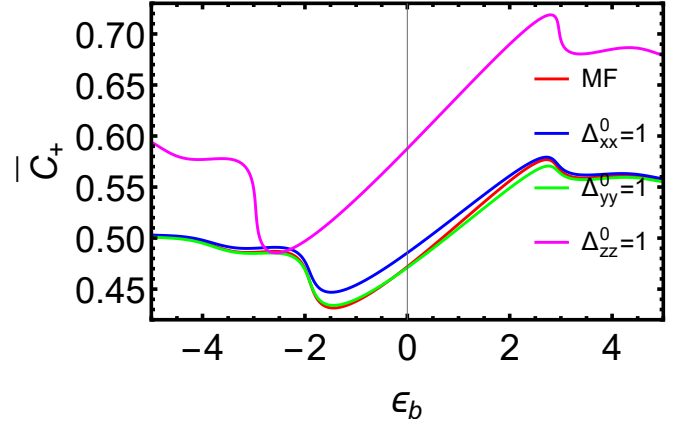


FIG. 13: Time-averaged condensate part ( $\bar{C}_{+}$ ) is controlled by detuning ( $\epsilon_b$ ), where the following fluctuations are represented by their respective colors: MF (—),  $\Delta_{xx}^0 = 1$  (—),  $\Delta_{yy}^0 = 1$  (—), and  $\Delta_{zz}^0 = 1$  (—).

### C. Why do the Resonance points shifts to the Positive Detuning Side?

#### 1. shifts due to magnetic field fluctuation

New resonance point ( $B_{\text{res}}$ ) due to magnetic field fluctuation ( $\delta B$ ) in  $\epsilon_b$  is [102],

$$B_0 = B_{\text{res}} + \delta B \quad (26a)$$

From definition of  $\epsilon_b$ , one obtains,

$$\epsilon_b = \epsilon_b^0 - \mu_{\text{co}} \delta B \quad (26b)$$

where,  $\epsilon_b^0 = \mu_{\text{co}}(B - B_{\text{res}})$ . So, From Eq. (26b), we obtain

$$\delta B = -\frac{\delta \Delta B}{\delta \mu_{\text{co}}} \quad (26c)$$

From definition of  $g$ , we obtain,

$$a(B) = \alpha g^2 \quad (27a)$$

where,  $\alpha = m/4\pi\hbar^2\Delta B\mu_{\text{co}}$ . On the other hand [103]

$$a(B) = a_{\text{bg}}\left(1 - \frac{\Delta B}{B - B_0}\right) \quad (27b)$$

Now, comparing both Eqs. (27a), and (27b), we obtain

$$B - B_0 = \Delta B(1 - \alpha\tilde{g}^2)^{-1} \quad (28a)$$

Since,  $\alpha\tilde{g}^2 = \left(1 - \Delta B/(B - B_0)\right)^2$ , and for positive scattering length in BEC make,  $\alpha\tilde{g}^2 < 1$ . Now, Eq. (28a), produces,

$$B - B_0 = \Delta B(1 + \alpha\tilde{g}^2) \quad (28b)$$

Now, Eq. (26c), generates

$$\delta B = -\Delta B(1 + \alpha\tilde{g}^2) \quad (29a)$$

which generates

$$B_{\text{res}} - B_0 = \Delta B(1 + \alpha\tilde{g}^2) = +ve \quad (29b)$$

So, the resonance point shifts right because of magnetic fluctuation or noise in the Feshbach detuning.

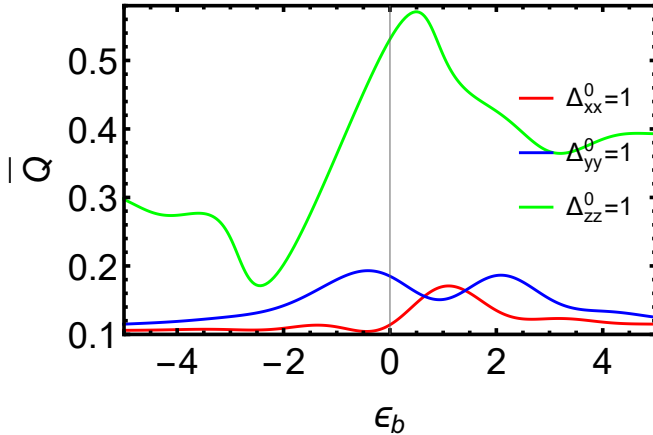


FIG. 14: Time-averaged quantum fisher information ( $\bar{Q}$ ) is controlled by detuning ( $\epsilon_b$ ) where the following variances are represented by their respective colors:  $\Delta_{xx}^0 = 1$  (—),  $\Delta_{yy}^0 = 1$  (—), and  $\Delta_{zz}^0 = 1$  (—).

## 2. shifts due to phase noise

When Feshbach coupling strength,  $\tilde{g}$  corrupted by Gaussian white noise,  $n_x$  then mean,  $\langle n_x \rangle = 0$ , and variances,  $\sigma_x^2 = \langle n_x^2 \rangle = \gamma_x/2$ , which generate

$$\langle (\tilde{g} + n_x)^2 \rangle = g^2 + \frac{\gamma_x}{2} \quad (30a)$$

From Eq. (28a), we obtain

$$B_{\text{res}} - B_0 = \Delta B\left(1 + \alpha(\tilde{g}^2 + \frac{\gamma_x}{2})\right) \quad (30b)$$

As a result of phase noise, the resonance point shifts to the right side.

## VII. CONCLUSION

In our recent work [48], we described how two bosonic atoms, when coupled via a Feshbach resonance, can bind to form a bosonic molecule. The energy gap between the unbound atomic pair and the bound molecular state is referred to as the detuning ( $\epsilon_b$ ). In our model, both the detuning and the Feshbach coupling are subject to Gaussian white noise. This two-mode system can be conveniently represented on a Bloch sphere, where the  $z$ -component of the Bloch vector ( $\hat{L}_z$ ) reflects the population imbalance between the atomic and molecular Bose-Einstein condensates (BECs), while  $\hat{L}_x$  and  $\hat{L}_y$  encode the real and imaginary parts of the coherence, respectively. To analyze the system's dynamics, we employ two complementary approaches. The first is the mean-field (MF) framework, which considers only the expectation values of the Bloch vector components,  $s_i = \langle \hat{L}_i \rangle$ . The second, more detailed, is the Bogoliubov Backreaction (BBR) method, which incorporates not just the means but also the second-order correlations specifically, the variances ( $\Delta_{ii}^0$ ) and covariances ( $\Delta_{ij}^0$ ). In that work [48], the  $\Delta_{ii}^0$  are treated as the variable parameters.

In this work, polarization and detuning are treated as the controlling variables of the same system, with  $\Delta_{ij}^0$  held fixed. As the noise preserves particle number (i.e.,  $\dot{N} = 0$ ), the relaxation behavior of the system can be characterized in terms of the longitudinal relaxation time ( $T_z$ ), associated with the decay of coherence ( $s_{\parallel}$ ), and the transverse relaxation time ( $T_{x-y}$ ), associated with the decay of polarization ( $s_z$ ), is characterized by the drift speed ( $|\dot{s}_z|$ ), which serves as a hallmark of the behavior of  $T_z$ . To understand the coherence relaxation dynamics, we investigate several key observables: (i) the time-averaged von Neumann entanglement entropy ( $\bar{S}_v$ ), (ii) the time-averaged fidelity ( $\bar{F}$ ), and (iii) the time-averaged Husimi Q distribution ( $\bar{H}$ ) when  $|s_z^0|$  serves as a variable. Moreover,  $T_z$  is found to decrease as the conversion efficiency ( $\Gamma$ ) increases. Additionally, we investigate the increase in  $T_{x-y}$  through several physical quantities: (i) the time-averaged participation ratio ( $\bar{P}_R$ ), (ii) the condensate fraction ( $\bar{C}_+$ ), and (iii) the quantum fisher information ( $\bar{Q}$ ) while  $\epsilon_b$  plays the role of variables.

The results that we obtain remain qualitatively unchanged in MF and BBR treatments: an indication that these are fundamental characteristics of the system, and are not affected by correlations and fluctuations.

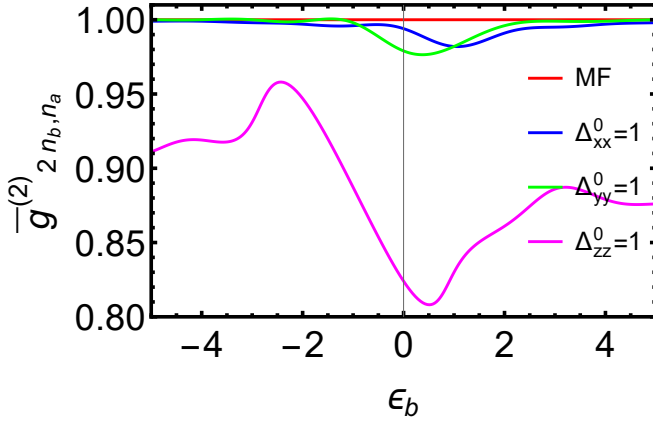


FIG. 15: Time-averaged 2nd-order correlations ( $\bar{g}_{2n_b, n_a}^{(2)}$ ) vs. detuning ( $\epsilon_b$ ), for all cases. We have: MF (—),  $\Delta_{xx}^0 = 1$  (—),  $\Delta_{yy}^0 = 1$  (—), and  $\Delta_{zz}^0 = 1$  (—).

#### Appendix A: Signature of closed system

The time-averaged second-order correlation function between atom-dimer states is defined as [86, 104]

$$\bar{g}_{2n_b, n_a}^{(2)} = \frac{\overline{2n_b n_a}}{\bar{n}_a \bar{n}_b} = 1 - \frac{\bar{\Delta}_{zz}}{2(1 - \bar{s}_z^2)} < 1. \quad (\text{A1})$$

Here,  $\bar{g}_{2n_b, n_a}^{(2)} < 1$  because coherent population transfer occurs, meaning that atoms and dimers are not created simultaneously; in other words, the creation of one species suppresses the formation of the other, as shown in Fig. (15). Here, we obtain the minima of this curve near resonance ( $\epsilon_b = 0$ ).

From expression of  $N$ , and  $L_z$ , we obtain  $N_a/N = (1 - s_z)/2$ , and  $2N_b/N = (1 + s_z)/2$  [69, 105]. So, time dependence of  $N_b(t)$  looks like

$$N_b(t) \approx \frac{N}{2} L_z(t) \quad (\text{A2})$$

where the constant part is not considered in the dynamics. If we model  $N_b(t) = N_b^0 e^{-t/T_b}$  and  $L_z(t) = L_z^0 e^{-t/T_z}$ , then  $T_b = T_z$ , where  $N_b^0$  and  $L_z^0$  are the amplitudes of  $N_b$  and  $L_z$ , respectively. Here,  $T_b$  represents the relaxation time of  $N_b$ . If we start from a fully molecularly polarized state, corresponding to the North Pole of the Bloch sphere, then the atomic and molecular populations evolve as

$$N_a(t) = N(1 - e^{-t/T_a}) \quad \text{and} \quad 2N_b(t) = N e^{-t/T_b} \quad (\text{A3})$$

Substituting these expressions into  $\dot{N} = 0$ , we find that  $T_a = T_b$  since the system is closed.

Note that in our system ( $^{87}\text{Rb}$ ), the atomic population increases while the molecular population decreases over time [105].

#### Appendix B: Expressions of frequency, damping rate and forces

From, Eq. (5b), we obtain the damping rate of Bloch vector components are:

$$\frac{1}{T_{\text{BBR}}^x} = \frac{\gamma_z}{2} \quad (\text{B1a})$$

$$\frac{1}{T_{\text{BBR}}^y} = 2\gamma_x(1 - 3s_z) + \frac{\gamma_z}{2} \quad (\text{B1b})$$

$$\frac{1}{T_{\text{BBR}}^z} = 2\gamma_x(1 - 3s_z) \quad (\text{B1c})$$

Now, the vivid expression of Eq. (5c) :

$$\omega_x^2 = 2c_1^2 \Delta_{zz} - (2c_1 s_z + c_2)^2 \quad (\text{B2a})$$

$$\begin{aligned} \omega_y^2 = & 2(c_1^2 - 9\gamma_x^2) - 9\gamma_x^2 \Delta_{zz} + (c_2 + 2c_1 s_z)^2 \\ & - 2\sqrt{2}\tilde{g}(6\gamma_x s_y + 3\sqrt{2}\tilde{g}s_z - 2c_1 s_x - \sqrt{2}\tilde{g}) \\ & + 6\gamma_x^2(1 + 3s_z)(1 - s_z) \end{aligned} \quad (\text{B2b})$$

$$\omega_z^2 = 2s_z \left( 2\sqrt{2}\tilde{g}c_1 s_x + \tilde{g}^2(2 - 3s_z) - 3\gamma_x(s_y + 3\gamma_x \Delta_{zz}) \right) \quad (\text{B2c})$$

From Eq. (5d) we obtain the intrinsic forces on Bloch vector components are:

$$\begin{aligned} F_x = & \Delta_{zz} \left( 9\gamma_x c_1 s_y + \frac{3\sqrt{2}\tilde{g}}{2} (3s_z c_1 + \frac{c_2}{2}) - \sqrt{2}\tilde{g} \right) \\ & - 2c_1(2c_1 s_z + c_2)\Delta_{zx} + 2\sqrt{2}\tilde{g}c_1 \Delta_{yy} \\ & + \Delta_{yz} \left( 3\gamma_x c_2 - \left( \frac{\gamma_z}{2} + 2\gamma_x c_1(2 + 9s_z) \right) \right) \\ & + (2c_1 s_z + c_2) \left( 2\gamma_x s_y(3s_z - 1) - \frac{\gamma_z s_y}{2} \right) \\ & - \frac{\tilde{g}}{\sqrt{2}}(1 + 2s_z - 3s_z^2) \\ & + 2c_1 s_y \left( 2\sqrt{2}\tilde{g}s_y - \gamma_x(1 + 2s_z - 3s_z^2) \right) \end{aligned} \quad (\text{B3a})$$

$$\begin{aligned} F_y = & \Delta_{yz} \left( 2 \left( 3\tilde{g}^2 - c_1(2c_1 s_z + c_2) \right) - 3\gamma_x \left( \frac{\gamma_z}{2} + 4\gamma_x(1 - 3s_z) \right) \right) \\ & - 2\sqrt{2}\tilde{g}c_1 \Delta_{xy} + \Delta_{zx} \left( c_1 \left( 2\gamma_x(1 - 3s_z) + \frac{\gamma_z}{2} \right) - 3\gamma_x(2c_1 s_z + c_2) \right) \\ & - 3\gamma_x \Delta_{zz} \left( \sqrt{2}\tilde{g}(1 - 3s_z)(\gamma_x + \frac{3}{2}) + c_1 s_x(1 + 2\gamma_x) \right) \\ & + 6\sqrt{2}\tilde{g}\gamma_x \Delta_{yy} + \frac{\gamma_z s_x}{2}(2c_1 s_z + c_2) \\ & + \gamma_x(1 + s_z)(1 - 3s_z) \left( \sqrt{2}\tilde{g}(1 - 3s_z) + 2c_1 s_x \right) \end{aligned} \quad (\text{B3b})$$

$$F_z = 3 \left( 4 \sqrt{2} \tilde{g} \gamma_x \Delta_{yz} + (\tilde{g}^2 - 2\gamma_x^2) \Delta_{zz} \right) - 2\tilde{g} \left( \sqrt{2} c_1 \Delta_{zx} + \sqrt{2} \left( c_2 s_x + s_y (2\gamma_x + \frac{\gamma_z}{2}) \right) + \tilde{g} \right) \quad (\text{B3c})$$

### Appendix C: Characteristic Polynomial Framework for System Stability

If,  $\Delta_{ij} = 0$ , then Eq. (4) generates the Jacobian matrix ( $J_{ij}$ ),

$$\begin{pmatrix} -\frac{\gamma_z}{2} & 2c_1 s_z + c_2 & 2c_1 s_y \\ -(2c_1 s_z + c_2) & 2\gamma_x(3s_z - 1) - \frac{\gamma_z}{2} & -2c_1 s_x - \sqrt{2}\tilde{g}(1 - 3s_z) \\ 0 & 2\sqrt{2}\tilde{g} & 2\gamma_x(3s_z - 1) \end{pmatrix} \quad (\text{C1})$$

Using the two equilibrium points, unstable (0, 0, 1) and stable (0, 0, -1/3), we obtain the characteristic equations are:

$$\left( \lambda + \frac{\gamma_z}{2} \right) \left( (\lambda - 4\gamma_x + \frac{\gamma_z}{2})(\lambda - 4\gamma_x) - 8\tilde{g}^2 \right) + k^2(\lambda - 4\gamma_x) = 0 \quad (\text{C2a})$$

$$\left( \lambda + \frac{\gamma_z}{2} \right) \left( (\lambda + 4\gamma_x + \frac{\gamma_z}{2})(\lambda + 4\gamma_x) + 8\tilde{g}^2 \right) + k^2(\lambda + 4\gamma_x) = 0. \quad (\text{C2b})$$

---

\* [avinaba.mukherjee@rediffmail.com](mailto:avinaba.mukherjee@rediffmail.com)

† [rdphy@caluniv.ac.in](mailto:rdphy@caluniv.ac.in)

- [1] P. Naidon, E. Tiesinga, and P. S. Julienne, Two-body transients in coupled atomic-molecular bose-einstein condensates, *Physical review letters* **100**, 093001 (2008).
- [2] M. Holland, J. Park, and R. Walser, Formation of pairing fields in resonantly coupled atomic and molecular bose-einstein condensates, *Physical Review Letters* **86**, 1915 (2001).
- [3] M. Gupta and K. R. Dastidar, Control of the dynamics of coupled atomic-molecular bose-einstein condensates: Modified gross-pitaevskii approach, *Physical Review A Atomic, Molecular, and Optical Physics* **80**, 043618 (2009).
- [4] G.-R. Jin, C. K. Kim, and K. Nahm, Quantum dynamics and statistical properties of atom-molecule bose-einstein condensates, *Physical Review A Atomic, Molecular, and Optical Physics* **72**, 045602 (2005).
- [5] T. Köhler, T. Gasenzer, and K. Burnett, Microscopic theory of atom-molecule oscillations in a bose-einstein condensate, *Physical Review A* **67**, 013601 (2003).
- [6] E. Braaten and H.-W. Hammer, Enhanced dimer relaxation in an atomic and molecular bose-einstein condensate, *Physical Review A Atomic, Molecular, and Optical Physics* **70**, 042706 (2004).
- [7] M. Mackie, A. Collin, and J. Javanainen, Comment on “stimulated raman adiabatic passage from an atomic to a molecular bose-einstein condensate”, *Physical Review A—Atomic, Molecular, and Optical Physics* **71**, 017601 (2005).
- [8] P. Drummond, K. Kheruntsyan, D. Heinzen, and R. Wynar, Stimulated raman adiabatic passage from an atomic to a molecular bose-einstein condensate, *Physical Review A* **65**, 063619 (2002).
- [9] B. J. Cusack, T. J. Alexander, E. A. Ostrovskaya, and Y. S. Kivshar, Existence and stability of coupled atomic-molecular bose-einstein condensates, *Physical Review A* **65**, 013609 (2001).
- [10] A. Vardi, V. Yurovsky, and J. Anglin, Quantum effects on the dynamics of a two-mode atom-molecule bose-einstein condensate, *Physical Review A* **64**, 063611 (2001).
- [11] J. Hope and M. Olsen, Quantum superchemistry: Dynamical quantum effects in coupled atomic and molecular bose-einstein condensates, *Physical Review Letters* **86**, 3220 (2001).
- [12] J.-J. Zhu and X. Chen, Fast-forward scaling of atom-molecule conversion in bose-einstein condensates, *Physical Review A* **103**, 023307 (2021).
- [13] A. P. Tonel, C. C. N. Kuhn, G. Santos, A. Foerster, I. Roditi, and Z. V. T. Santos, Classical and quantum analysis of a heterotriatomic molecular bose-einstein-condensate model, *Physical Review A Atomic, Molecular, and Optical Physics* **79**, 013624 (2009).
- [14] M. Mackie, A. Collin, and J. Javanainen, Comment on “stimulated raman adiabatic passage from an atomic to a molecular bose-einstein condensate”, *Physical Review A Atomic, Molecular, and Optical Physics* **71**, 017601 (2005).
- [15] T. G. Vaughan, K. Kheruntsyan, and P. Drummond, Three-dimensional solitons in coupled atomic-molecular bose-einstein condensates, *Physical Review A Atomic, Molecular, and Optical Physics* **70**, 063611 (2004).
- [16] K. Kheruntsyan and P. Drummond, Quantum correlated twin atomic beams via photodissociation of a molecular bose-einstein condensate, *Physical Review A* **66**, 031602 (2002).
- [17] E. Timmermans, P. Tommasini, M. Hussein, and A. Kerman, Feshbach resonances in atomic bose-einstein condensates, *Physics Reports* **315**, 199 (1999).
- [18] T. Köhler, K. Góral, and P. S. Julienne, Production of cold molecules via magnetically tunable feshbach resonances, *Reviews of modern physics* **78**, 1311 (2006).
- [19] M. Pigneur, T. Berrada, M. Bonneau, T. Schumm, E. Demler, and J. Schmiedmayer, Relaxation to a phase-locked equilibrium state in a one-dimensional bosonic josephson junction, *Physical review letters* **120**, 173601 (2018).
- [20] R. Gerritsma, A. Negretti, H. Doerk, Z. Idziaszek, T. Calarco, and F. Schmidt-Kaler, Bosonic josephson junction controlled by a single trapped ion, *Physical Review Letters* **109**, 080402 (2012).
- [21] T. Betz, S. Manz, R. Bücker, T. Berrada, C. Koller, G. Kazakov, I. E. Mazets, H.-P. Stimming, A. Perrin, T. Schumm, *et al.*, Two-point phase correlations of a one-dimensional bosonic josephson junction, *Physical review letters* **106**, 020407 (2011).
- [22] E. Boukobza, M. G. Moore, D. Cohen, and A. Vardi, Nonlinear phase dynamics in a driven bosonic josephson junction, *Physical review letters* **104**, 240402 (2010).
- [23] M. Albiez, R. Gati, J. Fölling, S. Hunsmann, M. Cristiani, and M. K. Oberthaler, Direct observation of tunneling and nonlinear self-trapping in a single bosonic josephson junction, *Physical review letters* **95**, 010402 (2005).
- [24] J. Tian, H. Qiu, G. Wang, Y. Chen, and L.-b. Fu, Measure synchronization in a two-species bosonic josephson junction, *Physical Review E—Statistical, Nonlinear, and Soft Matter Physics* **88**, 032906 (2013).
- [25] S. Wimberger, G. Manganelli, A. Brollo, and L. Salasnich, Finite-size effects in a bosonic josephson junction, *Physical Review A* **103**, 023326 (2021).

- [26] M. Pigneur and J. Schmiedmayer, Analytical pendulum model for a bosonic josephson junction, *Physical Review A* **98**, 063632 (2018).
- [27] J. Schurer, R. Gerritsma, P. Schmelcher, and A. Negretti, Impact of many-body correlations on the dynamics of an ion-controlled bosonic josephson junction, *Physical Review A* **93**, 063602 (2016).
- [28] K. Sakmann, A. I. Streltsov, O. E. Alon, and L. S. Cederbaum, Universality of fragmentation in the schrödinger dynamics of bosonic josephson junctions, *Physical Review A* **89**, 023602 (2014).
- [29] P. Buonsante, R. Burioni, E. Vescovi, and A. Vezzani, Quantum criticality in a bosonic josephson junction, *Physical Review A Atomic, Molecular, and Optical Physics* **85**, 043625 (2012).
- [30] M. Lapert, G. Ferrini, and D. Sugny, Optimal control of quantum superpositions in a bosonic josephson junction, *Physical Review A Atomic, Molecular, and Optical Physics* **85**, 023611 (2012).
- [31] M. Chuchem, K. Smith-Mannschott, M. Hiller, T. Kottos, A. Vardi, and D. Cohen, Quantum dynamics in the bosonic josephson junction, *Physical Review A Atomic, Molecular, and Optical Physics* **82**, 053617 (2010).
- [32] K. Sakmann, A. I. Streltsov, O. E. Alon, and L. S. Cederbaum, Quantum dynamics of attractive versus repulsive bosonic josephson junctions: Bose-hubbard and full-hamiltonian results, *Physical Review A Atomic, Molecular, and Optical Physics* **82**, 013620 (2010).
- [33] G. Mazzarella, L. Salasnich, A. Parola, and F. Toigo, Coherence and entanglement in the ground state of a bosonic josephson junction: From macroscopic schrödinger cat states to separable fock states, *Physical Review A Atomic, Molecular, and Optical Physics* **83**, 053607 (2011).
- [34] X. Jia, W. Li, and J. Liang, Nonlinear correction to the boson josephson-junction model, *Physical Review A Atomic, Molecular, and Optical Physics* **78**, 023613 (2008).
- [35] M. Abad, M. Guilleumas, R. Mayol, M. Pi, and D. M. Jezek, Phase slippage and self-trapping in a self-induced bosonic josephson junction, *Physical Review A Atomic, Molecular, and Optical Physics* **84**, 035601 (2011).
- [36] F. Binanti, K. Furutani, and L. Salasnich, Dissipation and fluctuations in elongated bosonic josephson junctions, *Physical Review A* **103**, 063309 (2021).
- [37] K. Kasamatsu, Uniformly frustrated bosonic josephson-junction arrays, *Physical Review A Atomic, Molecular, and Optical Physics* **79**, 021604 (2009).
- [38] G. Szirmai, G. Mazzarella, and L. Salasnich, Tunneling dynamics of bosonic josephson junctions assisted by a cavity field, *Physical Review A* **91**, 023601 (2015).
- [39] Y. Huang, Q.-S. Tan, L.-B. Fu, and X. Wang, Coherence dynamics of a two-mode bose-einstein condensate coupled with the environment, *Physical Review A* **88**, 063642 (2013).
- [40] L. Pitaevskii and S. Stringari, Thermal vs quantum decoherence in double well trapped bose-einstein condensates, *Physical Review Letters* **87**, 180402 (2001).
- [41] W. Wang, L. Fu, and X. Yi, Effect of decoherence on the dynamics of bose-einstein condensates in a double-well potential, *Physical Review A Atomic, Molecular, and Optical Physics* **75**, 045601 (2007).
- [42] A. Burchianti, F. Scazza, A. Amico, G. Valtolina, J. Seman, C. Fort, M. Zaccanti, M. Inguscio, and G. Roati, Connecting dissipation and phase slips in a josephson junction between fermionic superfluids, *Physical review letters* **120**, 025302 (2018).
- [43] J.-F. Mennemann, I. E. Mazets, M. Pigneur, H. P. Stimming, N. J. Mauser, J. Schmiedmayer, and S. Erne, Relaxation in an extended bosonic josephson junction, *Physical Review Research* **3**, 023197 (2021).
- [44] R. Gati and M. K. Oberthaler, A bosonic josephson junction, *Journal of Physics B: Atomic, Molecular and Optical Physics* **40**, R61 (2007).
- [45] D. Stefanatos and E. Paspalakis, Relaxation dynamics in a stochastic bosonic josephson junction, *Physics Letters A* **383**, 2370 (2019).
- [46] Y. Khodorkovsky, G. Kurizki, and A. Vardi, Decoherence and entanglement in a bosonic josephson junction: Bose-enhanced quantum zeno control of phase diffusion, *Physical Review A Atomic, Molecular, and Optical Physics* **80**, 023609 (2009).
- [47] H. Shen, X.-M. Xiu, and X. Yi, Atom-molecule-conversion system subject to phase noises, *Physical Review A Atomic, Molecular, and Optical Physics* **87**, 063613 (2013).
- [48] A. Mukherjee and R. Dasgupta, Relaxation dynamics in atomic-molecular bose condensates in the presence of gaussian noise, [arXiv:2507.18265v1](https://arxiv.org/abs/2507.18265v1) (2025).
- [49] F. Van Abeelen and B. Verhaar, Time-dependent feshbach resonance scattering and anomalous decay of a na bose-einstein condensate, *Physical review letters* **83**, 1550 (1999).
- [50] E. A. Donley, N. R. Claussen, S. T. Thompson, and C. E. Wieman, Atom-molecule coherence in a bose-einstein condensate, *Nature* **417**, 529 (2002).
- [51] N. R. Claussen, S. Kokkelmans, S. T. Thompson, E. A. Donley, E. Hodby, and C. Wieman, Very-high-precision bound-state spectroscopy near a 85 rb feshbach resonance, *Physical Review A* **67**, 060701 (2003).
- [52] N. R. Claussen, S. Kokkelmans, S. T. Thompson, E. A. Donley, E. Hodby, and C. Wieman, Very-high-precision bound-state spectroscopy near a 85 rb feshbach resonance, *Physical Review A* **67**, 060701 (2003).
- [53] G. Santos, A. Tonel, A. Foerster, and J. Links, Classical and quantum dynamics of a model for atomic-molecular bose-einstein condensates, *Physical Review A Atomic, Molecular, and Optical Physics* **73**, 023609 (2006).
- [54] G.-R. Jin, C. K. Kim, and K. Nahm, Quantum dynamics and statistical properties of atom-molecule bose-einstein condensates, *Physical Review A Atomic, Molecular, and Optical Physics* **72**, 045602 (2005).
- [55] G. Santos, A. Foerster, J. Links, E. Mattei, and S. R. Dahmen, Quantum phase transitions in an interacting atom-molecule boson model, *Physical Review A Atomic, Molecular, and Optical Physics* **81**, 063621 (2010).
- [56] J. Li, D.-F. Ye, C. Ma, L.-B. Fu, and J. Liu, Role of particle interactions in a many-body model of feshbach-molecule formation in bosonic systems, *Physical Review A Atomic, Molecular, and Optical Physics* **79**, 025602 (2009).
- [57] Y. Band, I. Tikhonenkov, and A. Vardi, Adiabatic molecular dynamics: two-body and many-body aspects, *Molecular Physics* **106**, 349 (2008).
- [58] E. Pazy, I. Tikhonenkov, Y. Band, M. Fleischhauer, and A. Vardi, Nonlinear adiabatic passage from fermion atoms to boson molecules, *Physical review letters* **95**, 170403 (2005).
- [59] I. Tikhonenkov, E. Pazy, Y. Band, M. Fleischhauer, and A. Vardi, Many-body effects on adiabatic passage through feshbach resonances, *Physical Review A Atomic, Molecular, and Optical Physics* **73**, 043605 (2006).
- [60] A. Auerbach, *Interacting Electrons and Quantum Magnetism* (Springer Verlag, 1994).
- [61] J. N. J. J. Sakurai, *Modern Quantum Mechanics*, 2nd ed. (Addison Wesley Publishing Company, 2011).



- [62] J. Liu, B. Liu, and L.-B. Fu, Many-body effects on nonadiabatic feshbach conversion in bosonic systems, *Physical Review A Atomic, Molecular, and Optical Physics* **78**, 013618 (2008).
- [63] B. Cui, L. Wang, and X. Yi, Atom-molecule conversion with particle losses, *Physical Review A Atomic, Molecular, and Optical Physics* **85**, 013618 (2012).
- [64] B. Liu, L.-B. Fu, and J. Liu, Shapiro-like resonance in ultracold molecule production via an oscillating magnetic field, *Physical Review A Atomic, Molecular, and Optical Physics* **81**, 013602 (2010).
- [65] C. W. Gardiner, Handbook of stochastic methods for physics, chemistry and the natural sciences, Springer series in synergetics (1985).
- [66] J. Anglin, Cold, dilute, trapped bosons as an open quantum system, *Physical review letters* **79**, 6 (1997).
- [67] J. Ruostekoski and D. F. Walls, Bose-einstein condensate in a double-well potential as an open quantum system, *Physical Review A* **58**, R50 (1998).
- [68] D. Witthaut, F. Trimborn, and S. Wimberger, Dissipation induced coherence of a two-mode bose-einstein condensate, *Physical review letters* **101**, 200402 (2008).
- [69] A. K. Saha, D. S. Ray, and B. Deb, Phase diffusion and fluctuations in a dissipative bose-josephson junction, *Physical Review E* **107**, 034141 (2023).
- [70] P. C. Deshmukh, *Quantum Mechanics*, 1st ed. (Cambridge University Press, 2023).
- [71] K. E. Strecker, G. B. Partridge, and R. G. Hulet, Conversion of an atomic fermi gas to a long-lived molecular bose gas, *Physical review letters* **91**, 080406 (2003).
- [72] J. Liu, L.-B. Fu, B. Liu, and B. Wu, Role of particle interactions in the feshbach conversion of fermionic atoms to bosonic molecules, *New Journal of Physics* **10**, 123018 (2008).
- [73] S. T. Thornton and J. B. Marion, *CLASSICAL DYNAMICS OF PARTICLES AND SYSTEMS*, 5th ed (THOMSON BOOKS/COLE, 2004).
- [74] T. W. B. Kibble and F. H. Berkshire, *CLASSICAL MECHANICS*, 5th ed (Imperial College Press, 2004).
- [75] J. R. Taylor, *Classical Mechanics* (University Science Books, 2005).
- [76] V. Barger and M. Olsson, *CLASSICAL MECHANICS: A MODERN PERSPECTIVE*, 2nd ed (McGRAW - HILL, INC, 1995).
- [77] A. Ghatak, *Optics*, 4th ed. (Tata McGRAW - HILL, 2008).
- [78] H. J. Pain, *The Physics of Vibrations and Waves*, 6th ed. (John Wiley & Sons, Ltd, 2005).
- [79] A. Bettini, *A Course in Classical Physics 4-Waves and Light* (Springer International Publishing, 2017).
- [80] J. Franklin, *Mathematical Methods for Oscillations and Waves* (Cambridge University Press, 2020).
- [81] J. Franklin, *Mathematical Methods for Oscillations and Waves* (Cambridge University Press, 2020).
- [82] F. Bloch, Nuclear induction, *Physical review* **70**, 460 (1946).
- [83] L. Viola, E. Fortunato, S. Lloyd, C.-H. Tseng, and D. Cory, Stochastic resonance and nonlinear response using nmr spectroscopy, *Physical Review Letters* **84**, 5466 (2000).
- [84] I. Marino, S. Raghavan, S. Fantoni, S. Shenoy, and A. Smerzi, Bose-condensate tunneling dynamics: Momentum-shortened pendulum with damping, *Physical Review A* **60**, 487 (1999).
- [85] K. E. Strecker, G. B. Partridge, and R. G. Hulet, Conversion of an atomic fermi gas to a long-lived molecular bose gas, *Physical review letters* **91**, 080406 (2003).
- [86] G.-R. Jin, C. K. Kim, and K. Nahm, Quantum dynamics and statistical properties of atom-molecule bose-einstein condensates, *Physical Review A Atomic, Molecular, and Optical Physics* **72**, 045602 (2005).
- [87] J. Liu, L.-B. Fu, B. Liu, and B. Wu, Role of particle interactions in the feshbach conversion of fermionic atoms to bosonic molecules, *New Journal of Physics* **10**, 123018 (2008).
- [88] W. Greiner, *Classical Mechanics: Systems of Particles and Hamiltonian Dynamics* (Springer, 2003).
- [89] S. H. Strogatz, *Nonlinear Dynamics and Chaos: With Applications to Physics, Biology, Chemistry, and Engineering* (Addison-Wesley, 1994).
- [90] M. O. Scully and M. S. Zubairy, *Quantum Optics* (Cambridge University Press, 1997).
- [91] C. P. Slichter, *Principles of Magnetic Resonance*, 3rd ed. (Springer, 1989).
- [92] C. Gardiner and P. Zoller, *Quantum noise: a handbook of Markovian and non-Markovian quantum stochastic methods with applications to quantum optics* (Springer Science & Business Media, 2004).
- [93] M. A. Nielsen and I. L. Chuang, *Quantum Computation and Quantum Information* (Cambridge University Press, 2000).
- [94] M. Schlosshauer, *Decoherence and the Quantum to Classical Transition* (Springer, 2007).
- [95] I. Bengtsson and K. Życzkowski, *GEOMETRY OF QUANTUM STATES An Introduction to Quantum Entanglement*, 2nd ed. (Cambridge University Press, 2017).
- [96] C. Gardiner and P. Zoller, *The Quantum World of Ultracold Atoms and Light*, Vol. 2nd (Imperial College Press, 2014).
- [97] L. F. Santos and M. Rigol, Onset of quantum chaos in one-dimensional bosonic and fermionic systems and its relation to thermalization, *Physical Review E—Statistical, Nonlinear, and Soft Matter Physics* **81**, 036206 (2010).
- [98] T. Pudlik, H. Hennig, D. Witthaut, and D. K. Campbell, Dynamics of entanglement in a dissipative bose-hubbard dimer, *Physical Review A Atomic, Molecular, and Optical Physics* **88**, 063606 (2013).
- [99] J. Liu, H. Yuan, X.-M. Lu, and X. Wang, Quantum fisher information matrix and multiparameter estimation, *Journal of Physics A: Mathematical and Theoretical* **53**, 023001 (2020).
- [100] Y. Huang, H.-N. Xiong, W. Zhong, Z.-D. Hu, and E.-J. Ye, Quantum-dynamical phase transition and fisher information in a non-hermitian bose-hubbard dimer, *Europhysics Letters* **114**, 20002 (2016).
- [101] G. Ferrini, D. Spehner, A. Minguzzi, and F. W. Heeking, Effect of phase noise on quantum correlations in bose-josephson junctions, *Physical Review A—Atomic, Molecular, and Optical Physics* **84**, 043628 (2011).
- [102] C. Chin, R. Grimm, P. Julienne, and E. Tiesinga, Feshbach resonances in ultracold gases, *Reviews of Modern Physics* **82**, 1225 (2010).
- [103] C. J. Pethick and H. Smith, *Bose-Einstein Condensation in Dilute Gases* (Cambridge University Press, 2008).
- [104] G. Kordas, D. Witthaut, P. Buonsante, A. Vezzani, R. Burioli, A. Karanikas, and S. Wimberger, The dissipative bose-hubbard model: Methods and examples, *The European Physical Journal Special Topics* **224**, 2127 (2015).
- [105] A. Motohashi and T. Nikuni, Particle-localized ground state of atom-molecule bose-einstein condensates in a double-well potential, *Physical Review A Atomic, Molecular, and Optical Physics* **82**, 033631 (2010).